

CrossMark
click for updatesCite this: *J. Mater. Chem. A*, 2015, 3,
6679Received 22nd December 2014
Accepted 4th February 2015

DOI: 10.1039/c4ta07053d

www.rsc.org/MaterialsA

Ag/white graphene foam for catalytic oxidation of methanol with high efficiency and stability†

Huijie Zhao,^{‡a} Jizhong Song,^{‡ab} Xiufeng Song,^b Zhong Yan^b and Haibo Zeng^{*ab}

Oxidation of methanol not only eliminates contamination due to typical volatile organic compounds (VOCs), but also provides clean energy. Here, we report Ag/white graphene foam to act as a catalyst for the oxidation reaction of methanol with both high conversion efficiency and high stability. The T_{50} and T_{95} of the Ag/white graphene foam catalyst are as low as 50 °C and 110 °C, almost half that of Ag/ γ -Al₂O₃ catalysts. Furthermore, when the temperature was fixed at 100 °C, the 93% conversion efficiency of the Ag/white graphene foam was maintained with a fluctuation of less than 2% over 50 hours, while the conversion efficiency of Ag/ γ -Al₂O₃ degraded sharply from 46% to 30%. Such outstanding catalytic performance of the Ag/white graphene foam is mainly attributed to the unique microstructure, especially the multi-level pores and few-layer atomically thin walls, which has been well confirmed by the SEM and TEM observations.

1 Introduction

Oxidative conversion of methanol has attracted great interest due to the demands of an environment-friendly and energy-saving society. Methanol, an important organic chemical raw material and clean fuel, is colorless, transparent, and easily transported. Methanol as the typical representative of volatile organic compounds (VOCs), can be used for direct methanol fuel cells (DMFCs) and fuelled vehicles (methanol gasoline, methanol diesel).^{1–6} However, it can cause serious environmental damage due to its toxicity and volatility. Therefore, reducing the pollution released by the VOCs (methanol) becomes a topic of great importance and can be improved by increasing the catalytic efficiency of VOC (methanol) conversion.^{7–11}

The conversion efficiency is mainly associated with the key catalyst, co-catalyst, catalyst support and the third-group compounds.¹² As for a specific key catalyst, the use of supported catalysts is an effective route for improving catalytic activity, and the effect of a catalyst support on the catalytic process should not be neglected. However, conventional catalyst supports such as alumina, silica and carbon materials cannot always fully meet the needs. For example, γ -Al₂O₃ with a surface area of 150–300 m² g⁻¹ is widely used as a catalyst support, but

it has poor thermal stability especially under conditions in which the feed gas contains water. In addition, γ -Al₂O₃ undergoes a phase change to α -Al₂O₃ when the temperature is increased to 800 °C. The phase transformation results significantly in the decrease of surface area, the closure of pores and the encapsulation of active catalytic sites. Other catalyst supports such as SiO₂ for example, have the disadvantages of poor alkali resistance, low mechanical strength and easy sintering reunion, and hence cannot meet the demands of a harsh environment.^{9,11,13–17} Therefore, it is a matter of urgency to find a novel catalyst support to boost catalytic oxidation in harsh environments. High specific surface area, high thermal conductivity, hydrophobic properties, and good stability are the desired factors to achieve this aim, but how to fabricate such a catalyst support is still a great challenge.

Here, we report Ag/white graphene foam for the oxidation of methanol with both a high conversion efficiency and high stability. Notably, the catalyst supports are composed of three-dimensional white graphene foams (the bulk material is composed of a low-dimensional boron nitride nanosheet, in order to facilitate the writing, called 3D BN) with multi-level pores, atomically thin walls, and a specific surface area of 681 m² g⁻¹. These structural features endow the white graphene foams with superior advantages in the field of catalyst supports, and hence the supported Ag catalysts exhibit good catalytic activity and stability. The T_{50} and T_{95} of Ag/white graphene foam catalysts are as low as 50 °C and 110 °C, respectively, almost half that of Ag/ γ -Al₂O₃ catalysts. Furthermore, when the temperature was fixed at 100 °C, the 93% conversion efficiency of the Ag/white graphene foam was maintained with a fluctuation of less than 2% over 50 hours, while the conversion efficiency of Ag/ γ -Al₂O₃ degraded sharply from 46% to 30%.

^aState Key Laboratory of Mechanics and Control of Mechanical Structures & College of Materials Science and Technology, Nanjing University of Aeronautics and Astronautics, Nanjing 210016, China. E-mail: zeng.haibo@njust.edu.cn

^bInstitute of Optoelectronics & Nanomaterials, College of Materials Science and Engineering, Nanjing University of Science and Technology, Nanjing 210094, China

† Electronic supplementary information (ESI) available. See DOI: 10.1039/c4ta07053d

‡ These authors contributed equally to this work.

2 Experiments

2.1 Synthesis methods

In a typical procedure, ammonia borane (AB) was supplied as the B and N source due to its stoichiometric ratio and appropriate decomposition performance, while thiourea was used as the vesicant in the reaction process for its function in increasing mutual cross-linking between the intermediate products, improving the yield. Thiourea and ammonia borane (AB) with different mass ratios (0 : 1–5 : 1) were loaded at the crucible, then placed into the central region of a high-temperature tubular furnace and heated to 1100–1400 °C under N₂. After 1–5 h of growth, the furnace was cooled to room temperature and the 3D BN products were synthesized.

The as-grown 3D BN (2 mg mL⁻¹) products were dissolved in poly(ethylene glycol) (PEG) by sonication and magnetic stirring. Then the AgNO₃ (2 mg mL⁻¹) was added to the solution under stirring and exposure to an ultraviolet lamp (254 nm) for 30 min. After washing and drying, we can obtain Ag/3D BN samples. The Ag/ γ -Al₂O₃ sample (Ag loaded on the γ -Al₂O₃ support) and the Ag/C BN sample (Ag loaded on the commercial BN support) were prepared using a similar method.

2.2 Catalytic performance test

All the catalytic oxidation experiments were performed in a conventional fixed bed continuous-flow reactor under atmospheric pressure. It consists of a stainless steel tube (9 mm i.d.) charged with the required amount of catalyst. An E-type thermocouple was placed in the center of the catalyst bed to control the furnace and record the reaction temperature. The volatile organic compound (VOC) laden gas was generated by bubbling air through the VOC saturators, and then carrying out further dilution with another gas stream before reaching the reaction bed. An O₂/N₂ stream through a methanol saturator was mixed with another O₂/N₂ stream. In each test, the molar ratio between O₂ and N₂ is controlled at 5%, 10% and 20%. The concentration of methanol in the feed was regulated in the range of 1000–4000 ppmv by adjusting the saturator temperature. 300 mg of catalyst was placed into the center of the reactor and the total flow rate was kept at 200 mL min⁻¹ with a corresponding gas hourly space velocity (GHSV) of 40 000 h⁻¹.

The reaction temperature varied from 20 to 250 °C. Prior to the activity studies, the catalyst was activated at 500 °C in O₂ for 2 h, and then cooled to room temperature before introducing methanol. All catalytic oxidations were performed in the steady-state condition and started at a temperature that ensured zero conversion of the methanol. The product stream was separated by a capillary column and the VOC concentrations in the effluent were determined by GC. When the composition and concentration of the VOCs in the inlet streams were varied, only water and CO₂ were detected in the methanol oxidation. No CO was detected in any experiment. Carbon mass balances were conducted for each set of experimental conditions and the methanol conversion and selectivity to oxidation byproducts were calculated and found to be within a relative error of less than 5%. The conversion efficiencies of the oxidation reactions

were calculated based on the production of CO₂. The reaction was also conducted under various flow rates to test the influence of mass-transfer resistance on the catalyst. No significant rate change was noted, meaning that the mass-transfer limitation was negligible.

2.3 Characterization and application

A field-emission scanning electron microscope (SEM, SU-4800, Hitachi Corp.) and a transmission electron microscope with an energy-dispersive X-ray analyzer (EDX) (TEM or HRTEM, Tecnai F30 S-TWIN, FEI Corp.) were used to investigate the morphology and crystalline structure of the as-prepared 3D BN and Ag/3D BN, respectively. X-ray diffraction (XRD, D8 Advance, Bruker Cu K α radiation ($\lambda = 1.5406 \text{ \AA}$)) and X-ray photoelectron spectroscopy (XPS, PHI QuanteraII, and Japan-US Nano Surface Analysis Instruments Corp.) were used to test the composition. A contact angle meter (OCA20, dataphysics) was used to measure the hydrophobic property of 3D BN. Specific surface area tests (N₂ adsorption–desorption isotherms, ASAP 2020M + C, American Micromeritics Corp.) were used to detect the Brunauer–Emmett–Teller (BET) surface area and non-local density functional theory (NLDFT) pore-size distribution of the as-prepared 3D BN. The N₂ physisorption isotherms were measured at 77 K. Prior to the measurement, the samples were outgassed in vacuum at 300 °C for 10 h. The BET specific surface area was calculated from the N₂ adsorption data in relative pressure ranging from 0.05 to 0.35. Due to the broad pore size distribution (PSD), ranging from micropores to mesopores, the NLDFT method was used to calculate the pore widths and pore size distributions (ASiQwin software). An ultraviolet spectrophotometer (UV-VIS, UV-3600, Shimadzu Corp.) was used to verify the appearance of silver nanoparticles on the 3D BN. A gas chromatograph (GC, GC7890A, Agilent Corp.) was used to assess the catalytic performance of the Ag/3D BN, Ag/ γ -Al₂O₃, and pure 3D BN.

3 Results and discussion

Firstly, the white graphene foams were synthesized through thermolysis of thiourea (CN₂H₄S) and ammonia borane (AB) (H₆BN) mixtures. The former acted as a vesicant to release a mass of gas during the formation of BN arising from the later raw materials. Fig. 1 presents the fabrication process of the Ag/white graphene foam catalysts. Under ultraviolet (UV) light irradiation, the color of pure AgNO₃, 3D BN and their mixed solutions were quite different, as show in Fig. 1a. The unchanged 3D BN poly(ethylene glycol) (PEG) solution shows the high stability of the 3D BN support under UV radiation. Compared with the slight yellow dyeing of the AgNO₃ PEG solution, the color of the AgNO₃/3D BN mixed solution obviously changed from white to dark brown, indicating that the 3D BN support has a great influence on the loading process. The color change is mainly caused by the reducibility of the PEG solution and the UV irradiation, through the reduction of the Ag ions to atoms *via* electron transfer.¹⁸

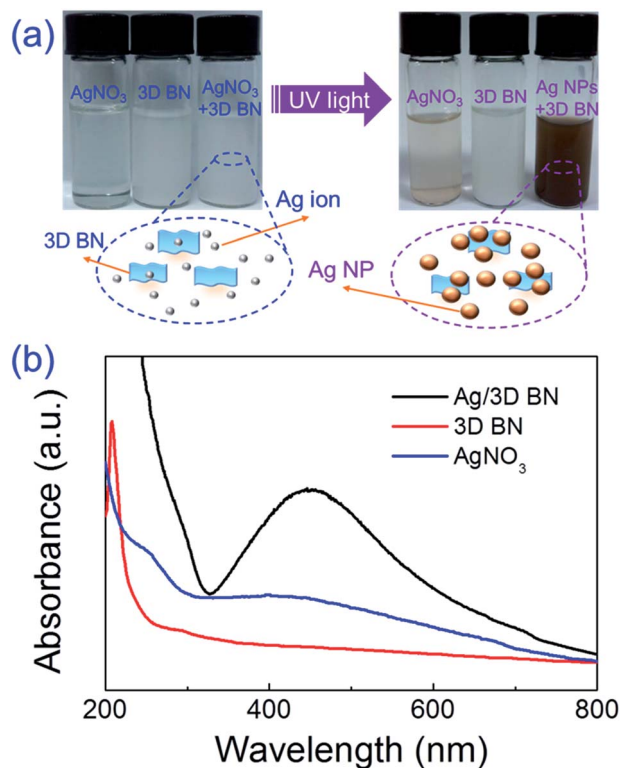


Fig. 1 (a) Photographs of pure AgNO₃, immersed 3D BN and their mixed solution before (left) and after (right) ultraviolet irradiation. (b) Comparison of the UV-vis absorption spectra of the three solutions.

The formation of Ag nanoparticles (Ag NPs) in the mixed solution was further confirmed by the comparison of the absorption spectra as shown in Fig. 1b. After irradiation, the local surface plasmon resonance (LSPR) peak of the Ag NPs at ~450 nm was very strong from the mixed solution of 3D BN and AgNO₃ PEG, very faint from the AgNO₃ PEG solution, and immeasurable from the 3D BN PEG solution.^{18,19}

The white graphene foams with and without Ag NPs were characterized in Fig. 2. Fig. 2a shows a photo of a white graphene foam with a length more than 10 cm, demonstrating the large amount prepared by the simple thermolysis method which can be realized in industrial applications. During the formation of the white graphene foam, the thiourea played an important role.^{20,21} It can promote the mutual crosslinking between the molecules of the transition state of AB, including polymeric aminoborane (PAB), (H₂BNH₂)_n, polyiminoborane (PIB), (HBNH)_n and borazine (B₃N₃H₆), *etc.*^{22,23} More importantly, thiourea can release a large amount of gas such as, H₂, N₂, NH₃, *etc.*, which initiated and gathered into bubbles and induced volume expansion, significantly improving the production and porosity of the boron nitride products. Therefore, we can get high quality 3D BN with a yield up to 62% compared to the raw materials of AB, far higher than previously reported data (40%).²⁴ The 3D network-like morphology can be clearly observed from the SEM image as shown in Fig. 2b. This network is composed of an irregular skeleton structure and typical flakes of the ultra-thin walls with a large planar size, as

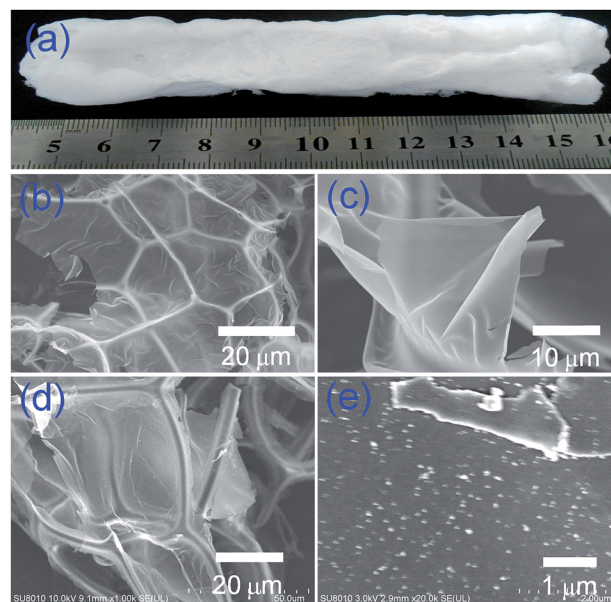


Fig. 2 (a) A photograph of the large amount of white graphene foam produced. SEM image of 3D BN (b and c) and Ag/3D BN (d and e). It is clearly seen that 3D BN consists of a network-like morphology (b) and has a large lamellar structure with ultra-thin walls (c). The Ag NPs are uniformly distributed on the 3D BN surface (d and e).

shown in Fig. 2c. Such a 3D structure with ultra-thin walls is conducive to improving the loading of silver onto the unit mass. In the process of loading the silver particles, the structure of the 3D BN support exhibits no obvious change even after several hours of ultrasound and magnetic stirring treatment, as shown in Fig. 2d, indicating the structure stability of 3D BN. Fig. 2e reveals the uniform distribution of Ag NPs on the 3D BN surface.

The detailed microstructure of the Ag/white graphene foam was further characterized by TEM, as shown in Fig. 3. The nanosized pores on the BN walls can be clearly seen in Fig. 3a. The white graphene foams were estimated to have a large specific surface area (SSA) of 681 m² g⁻¹ based on the Brunauer-Emmett-Teller (BET) method. The pore volume is 0.58 cm³ g⁻¹, and the corresponding bipolar pore size distribution of 1.5 and 32 nm were observed (ESI, Fig. S1†).²⁵ Fig. 3b confirms the three layer thickness of the lamellar structure, and the layer spacing is about 0.33 nm, which corresponds to the lattice spacing of the h-BN structure (002) plane.^{26,27}

Fig. 3c reveals that the Ag NPs are uniformly distributed on the BN surface. Their average diameter is about 5 nm and they have a size distribution from 2 to 10 nm (Fig. S2†). A typical HRTEM of a Ag NP is shown in Fig. 3d. Ag (112) and Ag (111) lattice fringes with spacing distances of 0.22 and 0.24 nm, respectively, are highlighted by the yellow lines.¹⁹ Fig. 3e shows the energy dispersive X-ray spectrum (EDX) mapping of B, N, and Ag elements, further confirming the formation of Ag catalysts on the ultrathin BN walls, which is consistent with the following X-ray photoelectron spectroscopy (XPS) and X-ray diffraction (XRD) measurements.

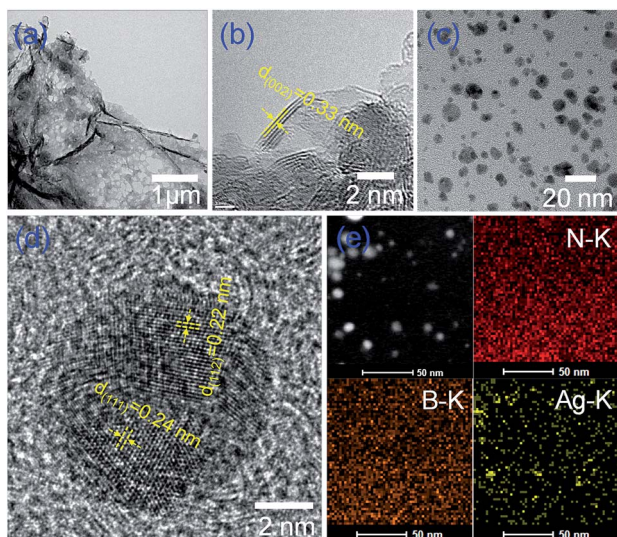


Fig. 3 TEM and HRTEM image of 3D BN (a and b, respectively) and Ag/3D BN (c and d, respectively). 3D BN exhibits a porous microstructure (a) and three layers of lamellar structure (b). TEM images (e) of the Ag NPs on 3D BN and the corresponding EDX elemental mapping of B, N and Ag.

The catalytic performance of the Ag/white graphene foam was characterized with the oxidation reaction of methanol as shown in Fig. 4. Prior to the reaction activity measurements, the catalysts were activated at 500 °C in O₂ for 2 h.^{28,29} Fig. 4a presents the temperature-dependent conversion efficiencies of methanol to CO₂. Comparing the catalytic activity of pure 3D BN with that of Ag/3D BN, we can claim that Ag is the primary active site in such an oxidation reaction. Comparing the catalytic performance of Ag/C BN (commercial BN) with that of Ag/3D

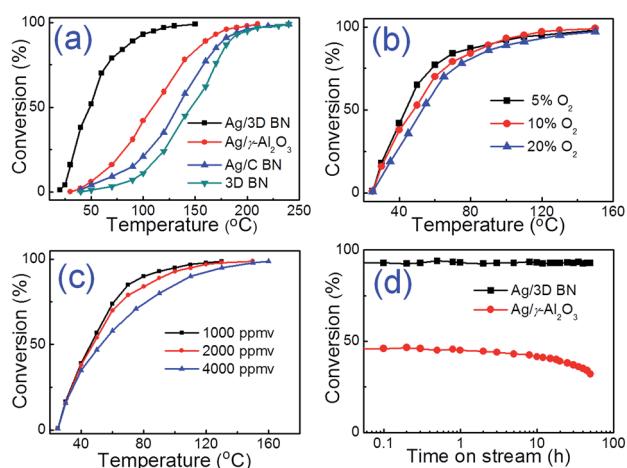


Fig. 4 (a) Temperature-dependent catalytic performance of Ag/3D BN, Ag/γ-Al₂O₃, Ag/C BN (commercial BN) and 3D BN, (10% O₂, 2000 ppmv methanol). (b) and (c) Effect of the O₂ (5%, 10%, 20% O₂, 2000 ppmv methanol) and methanol (10% O₂, 1000, 2000, 4000 ppmv methanol) concentration on the methanol conversion by Ag/3D BN. (d) Stability of Ag/3D BN, Ag/γ-Al₂O₃ catalysts for methanol oxidation at 100 °C.

BN, it can be said that the unique structural characteristics of the 3D BN support make it show obvious advantages over a commercial BN support. The Ag/3D BN exhibits outstanding catalytic activity, which is even better than that of conventional Ag/γ-Al₂O₃ catalysts. Generally, the activity of a given catalyst can be mainly characterized by two parameters, T_{50} and T_{95} , corresponding to the temperatures at which the conversion efficiency reaches 50% and 95%, respectively. The activities for the catalytic oxidation of several VOCs are summarized in Table 1, showing that the Ag/3D BN can be used as an effective catalyst. The light-off temperature (T_{50}) of Ag/3D BN is as low as 50 °C, and the temperature of T_{95} is only 110 °C. For comparison, those two values for Ag/γ-Al₂O₃ are 110 °C and 180 °C, far larger than those of Ag/3D BN. Fig. 4b and c show the effects of O₂ and methanol concentrations on the catalytic performance of Ag/3D BN. The conversion efficiency slightly fluctuated with the increase in both O₂ concentration and methanol concentration, which is typical behavior according to reaction dynamics.^{7,9,14,30}

Besides the activity, stability is also crucial for catalysts. Fig. 4d compares the catalytic stability of Ag/3D BN with Ag/γ-Al₂O₃ when the temperature is fixed at 100 °C. The Ag/3D BN catalysts exhibited a consistent conversion efficiency of around 93% with a fluctuation of less than 2% over the 50 hours of measurement. Besides the low conversion efficiency, the degradation of the Ag/γ-Al₂O₃ catalysts was so obvious that the conversion rate reduced firstly from 46.5% to 42% in the initial one hour and from 40% to 30% during the period from 10 to 50 hours. The initial degradation of the Ag/γ-Al₂O₃ catalysts was induced by the rapid accumulation of water vapor in the micropores due to its high water absorption, and capillary condensation. In sharp contrast, there was almost no such initial degradation for the Ag/3D BN catalysts, which may be attributed to the highly hydrophobic features of the white graphene foams with a hydrophobic angle of 131° (Fig. S3†). The second degradation of the Ag/γ-Al₂O₃ catalysts after a long time of oxidation reaction is usually attributed to the structural instability and weak thermal conductivity of γ-Al₂O₃.^{11,13,31} The absence of the long term degradation of the Ag/3D BN catalysts is due to the intrinsic properties of BN, such as the high structural stability, high thermal conductivity and hydrophobic properties of BN materials. It has been reported that BN can maintain stability in O₂-containing air at a much higher

Table 1 The comparison of different catalysts for VOC oxidation

Catalyst	VOC	T_{50} (°C)	T_{95} (°C)	Reference
Ag/3D BN	Methanol	50	110	This paper
Ag/γ-Al ₂ O ₃	Methanol	110	180	This paper
Ag/C BN	Methanol	134	195	This paper
6% Ag/γ-Al ₂ O ₃	Methanol	135	175	30
0.1% Pd/γ-Al ₂ O ₃	Methanol	187	239	30
0.1% Pt/γ-Al ₂ O ₃	Methanol	169	195	30
Pt/h-BN	Iso-hexane	170	300	11
Pt/γ-Al ₂ O ₃	Iso-hexane	260	350	11
0.37 wt% Pt/b-BN	Benzene	140	170	13
0.37 wt% Pt/a-BN	Benzene	140	175	13
Pt/Al ₂ O ₃	Benzene	240	280	13

temperature of about 950 °C, and that the thermal conductivity can reach up to 2000 W m⁻¹ K⁻¹ at room temperature.^{26,27}

The catalytic mechanism of Ag based catalysts has been controversial, but it is generally believed to have a certain relationship with oxygen. The formation of subsurface oxygen (O_γ) was considered necessary for the activation of Ag catalysts for methanol oxidation. Surface-bound atomic oxygen (O_α) preferentially led to the formation of complete oxidation products. The increase in the ratio of O_γ : O_α on the Ag surface would result in an increase in direct methanol oxidation. Recent studies have shown that the Ag–O interaction involving the formation of subsurface oxygen species exerts an important influence on the surface structure and, eventually, the catalytic properties of silver catalysts.^{28,29,32,33}

We used X-ray photoelectron spectroscopy (XPS) to detect the chemical states of Ag/3D BN to gain further understanding of the catalytic mechanism. The survey spectra in Fig. 5a reveals the co-existence of elements B, C, N, O, and Ag. The carbon detected is from surface contamination which is commonly observed by the sensitive XPS method. The detailed B and N peaks are shown in Fig. 5b, in which the main binding energies are located at 190.2 eV and 397.9 eV, respectively. Notably, compared with the symmetric N1s peak, the shape of the B1s peak shows obvious asymmetry with a shoulder at 192.1 eV, indicating the appearance of B–O bonds.³⁴ Meanwhile, the loading of Ag and the high temperature O₂ treatment do not have much impact on the B1s and N1s peaks. Only a slight movement of the peak position and shape is observed (Fig. S4†), indicating the presence of

interactions between boron nitride and silver, not that they are simply mixed together. Metal–support interactions have an important influence on the catalytic performance. Fig. 5c presents the high resolution Ag spectra of Ag/3D BN. Obviously, the oxygen activation shifts the Ag 3d_{5/2} binding energy from 368 to 367.4 eV, revealing that the Ag surface has been partially oxidized to Ag₂O.^{29,35–37} Such speculation about partial surface oxidation was further confirmed by the X-ray diffraction (XRD) measurements (Fig. S5†).

The mechanism of 3D BN/Ag catalytic methanol oxidation is described in Scheme 1. The high temperature oxygen treatment caused reconstruction of the Ag surface, forming subsurface oxygen and surface-bound atomic oxygen. The existence of subsurface oxygen facilitates the formation of active sites on silver catalysts, which could enhance the catalytic capability. Surface-bound atomic oxygen was inclined to form complete oxidation products. The 3D BN support provides a moderate surface area that can accommodate dispersed Ag metals, while still preserving the unique characteristics. Furthermore, the 3D BN support has the property of high thermal conductivity, temperature stability, acid–base resistance, and hydrophobicity (thus preventing moisture condensation on its surface), which greatly improves the performance of the catalyst. First, methanol and O₂ were adsorbed onto the surface of the silver then dissociated with improving reactivity, reducing the activation energy and increasing the reaction rate. Second, methanol can directly react with oxygen at a low temperature to produce H₂O and CO₂. Finally, H₂O and CO₂ molecules desorbed from the surface by diffusion. Then the adsorption–desorption cycle over the silver surface was continued.

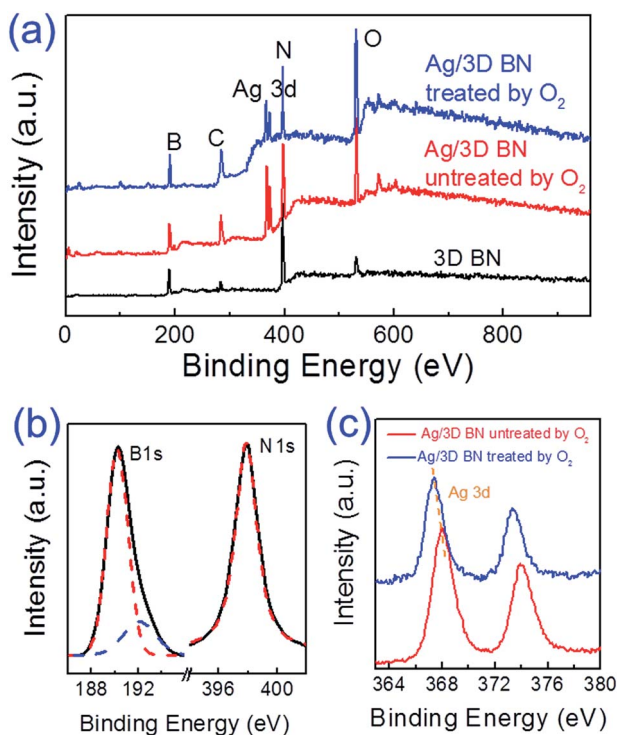
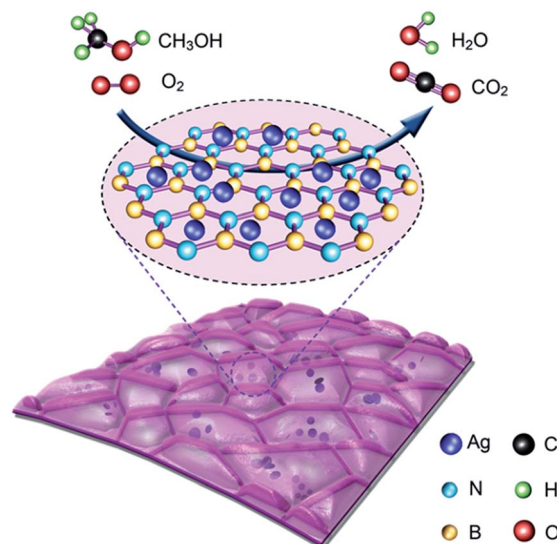


Fig. 5 (a) XPS spectra of the 3D BN and Ag/3D BN before and after O₂ treatment. (b) The detailed B1s and N1s spectra of 3D BN. (c) The detailed Ag 3d spectra of Ag/3D BN before and after O₂ treatment.

4 Conclusion

In summary, we apply white graphene foams to replace the usual γ -Al₂O₃ to act as a support of Ag catalysts for the high-



Scheme 1 Illustration of the reaction mechanism of Ag/3D BN catalytic methanol oxidation.

efficiency catalytic oxidation reaction of methanol. The white graphene foams were fabricated by a simple thermolysis method with a large amount of white graphene foam produced, and can be used as a catalyst support to effectively load uniform Ag NPs through UV irradiation. Compared with conventional Ag/ γ -Al₂O₃ catalysts, Ag/3D BN catalysts exhibited a much higher catalytic efficiency and better stability. The T₅₀ and T₉₅ of the Ag/3D BN catalysts are as low as 50 °C and 110 °C, almost half that of Ag/ γ -Al₂O₃ catalysts (110 °C and 180 °C). Over 50 hours of reaction, the 93% conversion efficiency of Ag/3D BN was maintained with a fluctuation of less than 2% when the temperature was fixed at 100 °C, while the efficiency of Ag/ γ -Al₂O₃ degraded sharply from 46% to 30%. Such an outstanding catalytic performance of the Ag/3D BN catalysts is mainly attributed to the interaction between the Ag NP and the 3D BN, the unique structural characteristics and the inherent quality of 3D BN. This kind of catalyst shows great potential for use in the field of environmental governance and energy applications.

Acknowledgements

This work was supported by the National 973 project from National Basic Research Program of China (2014CB931700), the National Natural Science Foundation of China (61222403), the Doctoral Program Foundation from the Ministry of Education of China (20123218110030), the Fundamental Research Funds for the Central Universities (30920130111017 and NE2012004) and the Opened Fund of the State Key Laboratory on Integrated Optoelectronics (IOSKL2012KF06), Natural Science Foundation for Youths of Jiangsu Province of China (BK20140787), China Postdoctoral Science Foundation funded project (2014M560425) and the Priority Academic Program Development of Jiangsu Higher Education Institutions.

Notes and references

- Q. Li, Y. Chen, J. R. Rowlett, J. E. McGrath, N. H. Mack and Y. S. Kim, *ACS Appl. Mater. Interfaces*, 2014, **6**, 5779–5788.
- M. Liu, Y. Lu and W. Chen, *Adv. Funct. Mater.*, 2013, **23**, 1289–1296.
- S. P. Jiang, Z. Liu and Z. Q. Tian, *Adv. Mater.*, 2006, **18**, 1068–1072.
- Z. Wen, J. Liu and J. Li, *Adv. Mater.*, 2008, **20**, 743–747.
- T. Yamaguchi, H. Zhou, S. Nakazawa and N. Hara, *Adv. Mater.*, 2007, **19**, 592–596.
- L. Feng, G. Gao, P. Huang, X. Wang, C. Zhang, J. Zhang, S. Guo and D. Cui, *Nanoscale Res. Lett.*, 2011, **6**, 551.
- J. H. Lee and D. L. Trimm, *Fuel Process. Technol.*, 1995, **42**, 339–359.
- M. Zhang, B. Zhou and K. T. Chuang, *Appl. Catal., B*, 1997, **13**, 123–130.
- J. C. S. Wu, Y.-C. Fan and C.-A. Lin, *Ind. Eng. Chem. Res.*, 2003, **42**, 3225–3229.
- H. Wu, H. Li, Y. Zhai, X. Xu and Y. Jin, *Adv. Mater.*, 2012, **24**, 1594–1597.
- J. C. S. Wu, Z. A. Lin, J. W. Pan and M. H. Rei, *Appl. Catal., A*, 2001, **219**, 117–124.
- V. M. Ehlinger, K. J. Gabriel, M. M. B. Noureldin and M. M. El-Halwagi, *ACS Sustainable Chem. Eng.*, 2014, **2**, 30–37.
- C. Lin, *J. Catal.*, 2002, **210**, 39–45.
- W. R. Schwartz, D. Ciuparu and L. D. Pfefferle, *J. Phys. Chem. C*, 2012, **116**, 8587–8593.
- L. S. Escandon, S. Ordonez, A. Vega and F. V. Diez, *Chemosphere*, 2005, **58**, 9–17.
- H. Zeng, C. Zhi, Z. Zhang, X. Wei, X. Wang, W. Guo, Y. Bando and D. Golberg, *Nano Lett.*, 2010, **10**, 5049–5055.
- X. Wang, D.-P. Yang, G. Huang, P. Huang, G. Shen, S. Guo, Y. Mei and D. Cui, *J. Mater. Chem.*, 2012, **22**, 17441–17444.
- H. Choi, S.-J. Ko, Y. Choi, P. Joo, T. Kim, B. R. Lee, J.-W. Jung, H. J. Choi, M. Cha, J.-R. Jeong, I.-W. Hwang, M. H. Song, B.-S. Kim and J. Y. Kim, *Nat. Photonics*, 2013, **7**, 732–738.
- Y. Lin, C. E. Bunker, K. A. Fernando and J. W. Connell, *ACS Appl. Mater. Interfaces*, 2012, **4**, 1110–1117.
- X. P. Hao, Y. Z. Wu, J. Zhan, J. X. Yang, X. G. Xu and M. H. Jiang, *J. Phys. Chem. B*, 2005, **109**, 19188–19190.
- X.-L. Meng, N. Lun, Y.-Q. Qi, J.-Q. Bi, Y.-X. Qi, H.-L. Zhu, F.-D. Han, Y.-J. Bai, L.-W. Yin and R.-H. Fan, *Eur. J. Inorg. Chem.*, 2010, **2010**, 3174–3178.
- G. Wolf, J. Baumann, F. Baitalow and F. P. Hoffmann, *Thermochim. Acta*, 2000, **343**, 19–25.
- D. Neiner, A. Karkamkar, J. C. Linehan, B. Arey, T. Autrey and S. M. Kauzlarich, *J. Phys. Chem. C*, 2009, **113**, 1098–1103.
- X. Wang, A. Pakdel, C. Zhi, K. Watanabe, T. Sekiguchi, D. Golberg and Y. Bando, *J. Phys.: Condens. Matter*, 2012, **24**, 314205.
- K. S. Sing, *Pure Appl. Chem.*, 1985, **57**, 603–619.
- D. Golberg, Y. Bando, C. C. Tang and C. Y. Zhi, *Adv. Mater.*, 2007, **19**, 2413–2432.
- X. Song, J. Hu and H. Zeng, *J. Mater. Chem. C*, 2013, **1**, 2952.
- Z. Qu, M. Cheng, W. Huang and X. Bao, *J. Catal.*, 2005, **229**, 446–458.
- X. Zhang, Z. Qu, F. Yu and Y. Wang, *J. Catal.*, 2013, **297**, 264–271.
- W. Wang, H. B. Zhang, G. D. Lin and Z. T. Xiong, *Appl. Catal., B*, 2000, **24**, 219–232.
- J. Mao, M. Deng, L. Chen, Y. Liu and Y. Lu, *Am. Inst. Chem. Eng.*, 2009, **56**, 1545.
- Z. P. Qu, W. X. Huang, M. J. Cheng and X. H. Bao, *J. Phys. Chem. B*, 2005, **109**, 15842–15848.
- W.-X. Li, C. Stampfl and M. Scheffler, *Phys. Rev. Lett.*, 2003, **90**, 256102.
- A. S. Nazarov, V. N. Demin, E. D. Grayfer, A. I. Bulavchenko, A. T. Arymbaeva, H. J. Shin, J. Y. Choi and V. E. Fedorov, *Chem.–Asian J.*, 2012, **7**, 554–560.
- L. Jin, K. Qian, Z. Jiang and W. Huang, *J. Mol. Catal. A: Chem.*, 2007, **274**, 95–100.
- W. Zhao, L. L. Feng, R. Yang, J. Zheng and X. G. Li, *Appl. Catal., B*, 2011, **103**, 181–189.
- W. W. He, X. C. Wu, J. B. Liu, K. Zhang, W. G. Chu, L. L. Feng, X. A. Hu, W. Y. Zbou and S. S. Me, *J. Phys. Chem. C*, 2009, **113**, 10505–10510.